ADVANCED OPTICAL MATERIALS
www.advopticalmat.de

Optically Pumped Lasing from Single Crystals of a Cyano-Substituted Thiophene/Phenylene Co-Oligomer

Hitoshi Mizuno, Takuro Maeda, Hisao Yanagi, Hiroyuki Katsuki, Mauro Aresti, Francesco Quochi, Michele Saba, Andrea Mura, Giovanni Bongiovanni, Fumio Sasaki, and Shu Hotta*

Since the first report on direct-current electroluminescence (EL) from an anthracene crystal by M. Pope et al. in 1963,[1] a number of researches have been actively conducted to develop organic light-emitting devices. After commercialization of organic EL, organic semiconductor laser is going to be one of future research targets. In order to realize an electrically pumped organic laser, molecular materials with high carrier mobility, emission efficiency, and stability are required. Although there are few organic materials satisfying all these conditions, thiophene/phenylene co-oligomers (TPCOs)[2–4] are most promising candidates owing to their robustness and excellent semiconducting properties.[5–7] In particular, high emission gain coefficients have been obtained based on the self-waveguiding light confinement due to high refractive indices in the TPCO crystals.[8] Longitudinal multimode lasing has been reported for several TPCOs by using a pair of parallel facets of the crystal as a Fabry–Pérot (F-P) resonator.[8] Moreover, spectrally narrowed emission has been observed from an organic light-emitting field-effect transistor (FET) with a single-crystal TPCO under AC gate operations.[9]

In order to achieve p-n junction type EL and FET devices, crystallization of both p-and n-types is necessary. Most of the TPCOs so far studied are p-type and are crystallized in thin platelet morphology. For example, in the monoclinic crystal of 2,5-bis(4-biphenylyl)thiophene (BP1T), the molecules align almost perpendicular to the crystal face.[10,11] Since the π-electronic transition dipole between the highest occupied and lowest unoccupied molecular orbitals (HOMO and LUMO, respectively) is parallel to the molecular axis, those monoclinic crystals result in low-threshold lasing due to the effective stimulated emission with the transverse magnetic (TM) mode.[12] By introducing methoxy groups at the molecular terminal of BP1T, 2,5-bis(4′-methoxybiphenyl-4-yl)thiophene (BP1T-OMe) changes to crystallize in an orthorhombic form in which all molecules perfectly stand upright to the crystal face.[13] This upright orientation is the most favorable for the TM-mode lasing in the platelet crystal.

Besides such crystallographic modification, the substituents into the TPCO molecule also change the p/n conduction types. Introduction of electron-withdrawing groups at the molecular terminal increases an electron-accepting nature resulting from lowered π electronic energies. Yamao et al. have confirmed the n-type conduction from a light-emitting FET device with vapor-grown crystals of 1,4-bis{5-[4-(trifluoromethyl)phenyl]thiophen-2-yl}benzene (AC5-CF_3).[14] By introducing trifluoromethyl groups, the HOMO/LUMO energies of AC5-CF_3 are deepened by 0.35 and 0.41 eV, respectively, in comparison to those of unsubstituted AC5 as demonstrated by the density functional theory (DFT) calculations.[15] In this study, we chose substitution into BP1T with cyano groups which are stronger electron-withdrawing than trifluoromethyl groups.[16,17] The HOMO and LUMO energy levels of 2,5-bis(4′-cyanobiphenyl-4-yl)thiophene (BP1T-CN)[4] are deepened by 0.48 and 0.65 eV, respectively with respect to those of unsubstituted BP1T (Figure S1). In contrast to the elevation of HOMO and LUMO energies by 0.20 and 0.19 eV, respectively, for the p-type BP1T-OMe, stronger n-type conduction is expected for BP1T-CN. While optically pumped lasing has been extensively investigated for p-type TPCO crystals,[18,19] there is no report for those n-type TPCOs so far. Here we investigated the optically pumped lasing from single crystals of a new derivative of BP1T-CN.

First, we characterized a crystal structure of BP1T-CN grown from a vapor phase. A fluorescence micrograph of a representative BP1T-CN crystal is shown in **Figure 1**(a). The crystal is blue-green-emitting with a fluorescence maximum at λ = 500 nm under ultraviolet (UV) excitation (Figure S2). As compared to fluorescence images of typical p-type TPCO crystals (Figure S3), remarkable differences appear in the BP1T-CN crystal: the crystal shape is typically rod-like instead of thin plate-like. The emission is enhanced at the both ends of the rod instead at all edges of the thin plate. The fluorescence is radiated also from the top face of the rod crystal (Figure 1(a)) whereas no fluorescence is seen in

H. Mizuno, T. Maeda, Prof. H. Yanagi, Prof. H. Katsuki
Graduate School of Materials Science
Nara Institute of Science
and Technology (NAIST), 8916-5
Takayama, Ikoma, Nara 630-0192, Japan
E-mail: mi-hitoshi@ms.naist.jp
M. Aresti, Dr. F. Quochi, Dr. M. Saba, Prof. A. Mura,
Prof. G. Bongiovanni
Dipartimento di Fisica
Università di Cagliari
SLACS-INFM/CNR
I-09042, Monserrato, Italy
Dr. F. Sasaki
Electronics and Photonics Research Institute
National Institute of Advanced Industrial Science
and Technology (AIST)
1-1-1 Umezono, Tsukuba, Ibaraki 305-8568, Japan
Prof. S. Hotta
Department of Macromolecular Science and Engineering
Graduate School of Science and Technology
Kyoto Institute of Technology
Matsugasaki, Sakyo-ku, Kyoto 606-8585, Japan

DOI: 10.1002/adom.201400083

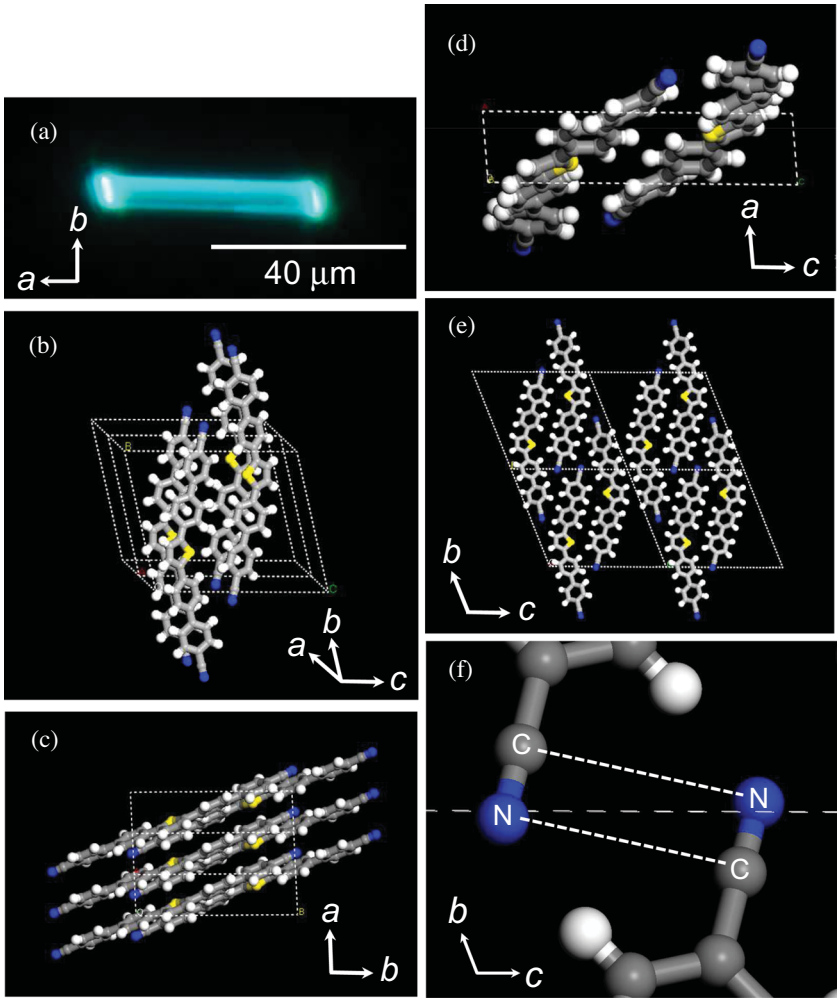

Figure 1. (a) A fluorescence micrograph of a rod-like crystal of BP1T-CN taken under ultraviolet excitation (λ_{ex} = 365 nm) using a mercury lamp. (b) Three-dimensional molecular packing of BP1T-CN crystal. (c) Crystal structure of BP1T-CN with projections on the *ab*-plane. (d) Crystal structure of BP1T-CN with projections on the *ac*-plane. (e) Molecular packing projected on the *bc*-plane. (f) Enlarged structure showing atomic interactions between carbon and nitrogen of the adjacent cyano groups.

the platelet face (Figure S3). In the typical TPCO crystals, the molecules stand upright against the crystal plane. Light emission from the molecules propagates along the crystal waveguide, and emits from the crystal edges (Figure S3). Those different features in light emission are ascribed to a unique crystal structure of BP1T-CN as shown in Figure 1(b)–(f). X-ray diffraction (XRD) analysis resulted in a triclinic form with P-1, a = 3.84, b = 16.15, c = 18.02 Å, α = 111.87, β = 94.27, γ = 90.43°, Z = 2 (CCDC registration code 897042). This triclinic structure, which has never been found for other TPCO crystals, is characterized by the molecular alignment of BP1T-CN in the *bc*-plane as shown in Figure 1(e). The bent-shaped molecules are intertwined each other with the molecular planes lying in the *bc*-plane. This peculiar packing is caused by Coulomb interaction between the carbon and nitrogen atoms in the two cyano groups of the adjacent molecules as shown in Figure 1(f). In the unsubstituted BP1T crystal, van der Waals interaction between π-electronic molecular frameworks governs its thin plate-like morphology with standing packing in the *ab*-plane.[20] By contrast, the *ab*-plane of the rod-like BP1T-CN crystal is formed by the obliquely lying molecules which are piled up by van der Waals interaction along the *a*-axis (Figure 1(c)). Consequently, the BP1T-CN crystal typically grows in rod-like morphology elongating along the *a*-axis as shown in Figure 1(a). XRD analysis determined that the top surface and the side facets of the crystal are assigned to the (025), (1-1-3) and (010) planes, respectively (Figure S4).

According to the determined crystal structure, the BP1T-CN molecular axes in the rod-like crystal are tilting by 62.4° against the crystal surface of the (025) plane (Figure S4(b)). The resulting oblique orientation of the transition dipole causes fluorescence radiation from the top (025) surface. This orientation seems to be unfavorable for light confinement in the crystal cavity since the emitted light is leaked from the top face. However, the bright emission at the both edges of the rod-like crystal indicates that the rod-like crystal acts as an optical waveguide along the *a*-axis. The transition dipoles piling up with an angle of 70.4° against the *a*-axis (Figure 1(c)) is favorable for light propagation along the rod axis. As a consequence, light amplification occurs along the rod direction (*a*-axis) with high stimulated emission rate under inverted population generated by short pulse excitation, as demonstrated below.

Figure 2(a) shows excitation density dependence of photoluminescence (PL) spectra taken from the short edges of the rod-like BP1T-CN crystal under optical pumping (λ_{ex} = 397 nm) at room temperature. At low excitation densities, broad emission bands appear around λ = 500 and 530 nm which are assigned to vibrational sidebands of the 0-1 and 0-2 progressions, respectively.[11] Due to the antiparallel exciton coupling between the adjacent molecules piled up along the *a*-axis, the lowest 0-0 transition is forbidden as same as other TPCO crystals.[11] With increasing excitation density up to 109 μJ/cm^2, the 0-1 band intensity increases linearly as shown in Figure 2(b). At an excitation density above a threshold of 138 μJ/cm^2, the spectrum changes to a typical feature of amplified spontaneous emission (ASE). The 0-1 emission is amplified into a gain-narrowed band with a full width at half maximum (FWHM) of ~7 nm and its intensity is nonlinearly increased. In order to understand the origin of higher threshold than other organic materials,[21,22] an absorption cross-section (Figure S2(b)) was estimated by the following relationship and absorption spectrum (Figure S2(a)): $\tau = n\sigma d$ (τ: optical density, n: molecular density, σ: absorption cross-section, d: crystal thickness). Although the in-plane long molecular axis of the BP1T-CN allows for efficient optical excitation, the effective absorption cross-section

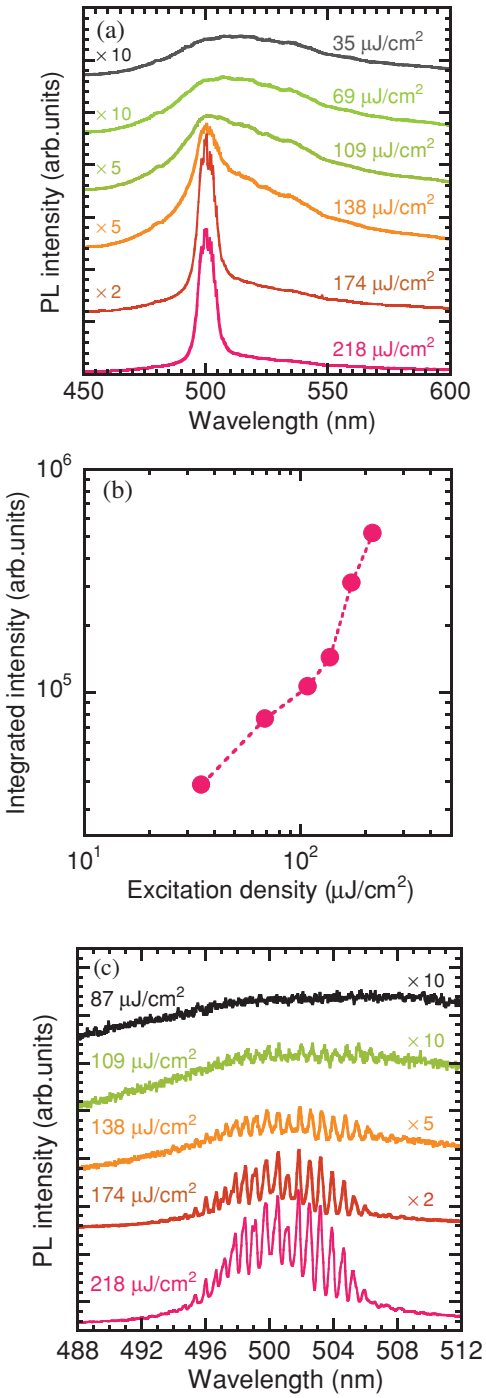

Figure 2. (a) Excitation density dependence of PL spectra of the BP1TCN rod-like crystal measured with a spectral resolution of 0.8–0.9 nm. (b) Excitation density dependence of the integrated 0-1 band intensity. (c) Excitation density dependence of the 0-1 band PL spectra measured with a spectral resolution of 0.2–0.3 nm.

per molecule at the pumping wavelength ($<10^{-18}$ cm^2) is smaller than the values (10^{-17}–10^{-16} cm^2) reported for other organic materials.[23,24] The smaller σ gave rise to the higher threshold. Figure 2(c) shows excitation density dependence of the 0-1 band PL spectra measured with a spectral resolution of 0.2–0.3 nm. As the excitation density is increased above the threshold, laser oscillations appear at the 0-1 band. These longitudinal multimodes are ascribed to the F-P resonation in the rod-like crystal cavity with the mirror facets in the rod ends. This F-P lasing was stably observed without quenching in air at room temperature. We calculated a group refractive index n_g of the BP1T-CN crystal according to the relationship, $n_g = 1/2L\Delta\nu$, where L is the distance between a pair of the parallel facets, and $\Delta\nu$ is the frequency interval of the lasing modes. n_g of ~4.18 was obtained by substituting $\Delta\nu = 27.8$ cm^{-1} evaluated from the Fourier transform of Figure 2(c) and $L = 43$ μm of the crystal shown in Figure 1(a). The Q factor estimated from the $\Delta\nu$ and the FWHM of the lasing peak is ~1860. These parameters of n_g and Q factor demonstrate that the BP1T-CN crystal is an excellent gain medium as similar as other TPCO crystals.

To evaluate a performance as laser media of the rod crystal, we determined the net gain coefficient of the 0-1 band emission along the rod axis direction by a variable stripe length method (Figure S5). The 0-1 emission intensity as a function of excitation length was fitted according to the equation, $I = I_{sp}[e^{g}\text{-}1]/g$, where I_{sp} is the intensity of spontaneous emission, g is the net gain coefficient, and l is the excitation stripe length. The net gain coefficient of the 0-1 band is determined to be 40 cm^{-1} at an excitation density of 236 μJ/cm^2. This value is considerably larger than that of other oligomer materials.[21,25] This high net gain coefficient is attributed to the efficient stimulated emission based on the one-dimensional stacking of the BP1T-CN molecules along the *a*-axis of the rod-like crystal.

Figure 3 shows the lasing spectra from other BP1T-CN crystals with different crystal size and morphology. Lasing spectrum in Figure 3(a) was taken from a rod-like crystal with a smaller size (L ~ 20 μm) at an excitation density of 264 μJ/cm^2 (lasing threshold $I_{th} = 132$ μJ/cm^2). Since the mode interval of the laser oscillation is inversely proportional to the resonator lengths, $\Delta\nu$ (=50.2 cm^{-1}) became larger than that in Figure 2(c), resulting in a decrease of number of modes. Besides the rod-like morphology, BP1T-CN was also grown in a platelet-like crystal with a lozenge or parallelogram as shown in the inset of Figure 3(b). The crystal surface with the quasi-lozenge shape was assigned to the (001) plane according to the XRD measurements (Figure S6). In this quasi-lozenge crystal, the molecular axis is tilting by 22.0° against the crystal surface of the (001) plane (Figure S6(b)). This slightly tilted orientation of the molecules seems to be suitable for surface-emitting. However, this crystal also exhibited in-plane lasing as shown in the spectrum, while surface-emitting laser was not achieved. The in-plane lasing threshold I_{th} and Q factor are 178 μJ/cm^2 and ~910, respectively. Taking into account of $\Delta\nu$ of 66.6 cm^{-1} and L of 17 μm, n_g of ~4.42 is obtained. This n_g value is comparably large as similar as that observed for the rod-like crystal. As a consequence, the closely packed stacking along the *a*-axis enhances the in-plane lasing rather than the surface emitting lasing.

To gain further insight into the excited-state dynamics of the platelet crystal of BP1T-CN in the lasing regime, pump-probe differential transmission ($\Delta T/T$) spectroscopy[26,27] was performed. The pump-probe spectroscopy is a technique of the high resolution time-resolved optical measurements using a pulsed laser. In the $\Delta T/T$, the ΔT equals to $T'\text{-}T$, where T and

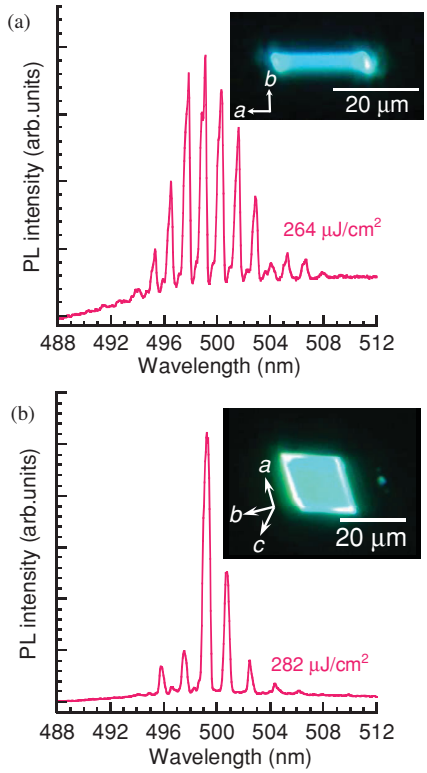

Figure 3. (a) Lasing spectrum of BP1T-CN rod-like crystal. (b) Lasing spectrum of BP1T-CN platelet-like crystal. These spectra were measured with a spectral resolution of 0.2–0.3 nm. The insets show the fluorescence micrographs of rod-like crystal and platelet-like crystal, respectively.

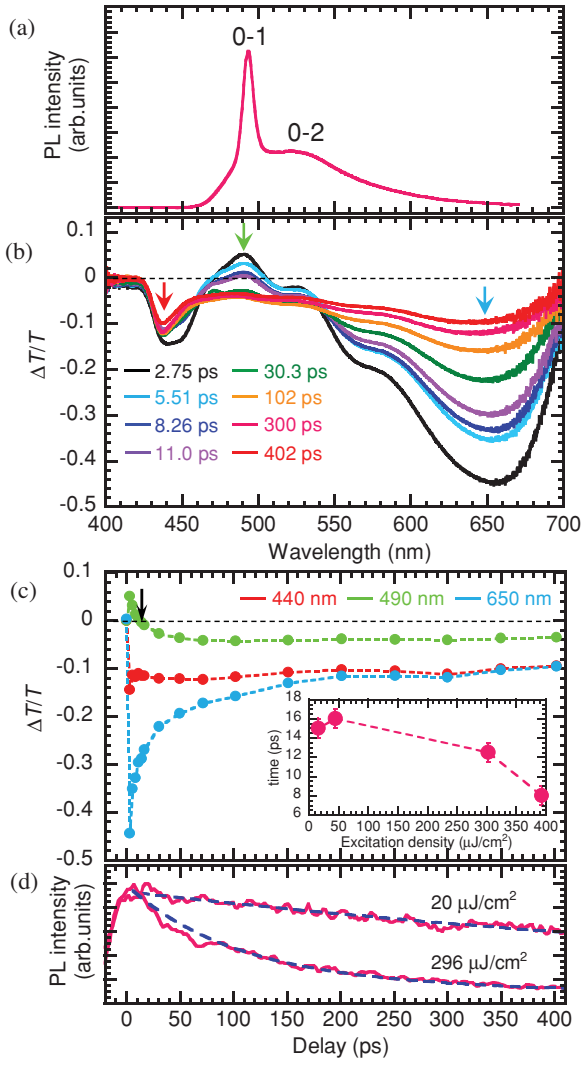

Figure 4. (a) ASE spectrum measured at an excitation density of 229 μJ/cm^2. (b) $\Delta T/T$ spectra for various pump-probe delays measured at an excitation density of 303 μJ/cm^2. (c) $\Delta T/T$ time traces of components of 440, 490 and 650 nm in $\Delta T/T$ spectra. The inset shows the excitation density dependence of zero crossing ($\Delta T/T = 0$) time (indicated by the arrow) at the ASE peak wavelength (490 nm). (d) PL time traces of 0-1 emission band measured at 20 and 296 μJ/cm^2.

T are the transmittance before optical excitation and at a time delay Δt after excitation, respectively. Immediately after photoexcitation, the $\Delta T/T$ spectrum probed at an excitation density of 303 μJ/cm^2 (above the threshold) exhibits a positive ($\Delta T/T > 0$) band extending from ~470 nm to ~500 nm. Two main photoinduced absorption bands (PA, $\Delta T/T < 0$) appeared at 440-450 nm and 660 nm, respectively (**Figure 4**). The peak of positive band at ~490 nm coincides with the ASE peak observed in the emission spectrum. Thus, the peak located at ~490 nm is attributed to stimulated emission of primary photoexcitations (singlet excitons). Stimulated emission is short-lived: the $\Delta T/T$ signal at 490 nm crosses zero value after a time of the order of 10 ps, turning negative thereafter. Such very short optical gain lifetime, which is actually shortened with increasing excitation density (inset of Figure 4(c)), is traced back to the high stimulated emission rate promptly sustained by singlet excitons in the regime of ASE emission. A first transient in the $\Delta T/T$ response with a ~30–40 ps characteristic time is fully ascribed to singlet excitons. This transient results probably from a combination of stimulated emission and singlet-singlet annihilation processes and is characterized by rather complementary dynamics at 490 and 650 nm. These results suggest that singlet excitons give rise not only to stimulated emission right below the ground-state absorption onset (Figure S2), but also to excited-state absorption at longer wavelengths. Figure 4(d) shows the PL time traces of the 0-1 emission band measured at 20 and 296 μJ/cm^2. At 20 μJ/cm^2 well below the threshold, the time decay profile is characterized by spontaneous decay with a lifetime of 900 ps. The profile at 20 μJ/cm^2 is dominated by a monomolecular process. At 296 μJ/cm^2 above the threshold, the profile is characterized by two components of 100 ps and 700 ps. Above the threshold, nonlinear processes dominate the singlet recombination dynamics in the ASE regime. Upon completion of the initial transient, long-lived PA features are characterized by a narrow band peaked at 440 nm. A broad band peaked at 650 nm is slightly blueshifted with respect to the PA band observed right after photoexcitation, and the PA band became a rather spectrally flat signal. The lifetime of component of 650 nm is much longer than the examined probe delay range (450 ps). This long-lived PA bands are tentatively assigned to a combination of populations of triplet exciton and polaron states. The PA signal at 440 nm practically shows a prompt response to the pump pulses, hinting possible ultrafast dissociation of a population of

singlet excitons into polaron pairs (with consequent ultrafast triplet formation) via singlet-singlet annihilation, or as an extrinsic process assisted by crystal structure disorder.[27]

The existence of a long-lived PA signal spectrally overlapped with optical gain is expected to be the main factor limiting the lasing performance of BP1T-CN crystals in the nanosecond pulsed regime, where the pump pulse duration is comparable to or longer than the excited-state lifetime. Nevertheless, the overall optical gain performance in the ultrafast pumping regime is insensitive to long-lived PA and can be assessed on the simple basis of the prompt stimulated emission. For a nominal crystal thickness of 3 μm used in this pump-probe experiment, a $\Delta T/T$ signal value of ~0.025 (linearly interpolated at the ASE threshold) allows to estimate material gain to be ~80 cm^{-1} in the upright direction (*a*-axis). Given that the threshold net gain in the crystal waveguide is zero, and further assuming that optical gain is fully confined within the crystal, optical propagation losses in the BP1T-CN crystal are inferred to lie in the 80 cm^{-1} range. Consequently, the waveguide gain of 40 cm^{-1} obtained at the excitation density of 236 $\mu J/cm^2$ in the rod crystal (Figure S5) results in the material gain of ~120 cm^{-1}. This high gain performance of the BP1T-CN crystal could be more efficiently utilized by improving the cavity structure and reducing the optical loss towards electrically pumped lasing.

In conclusion, we observed room temperature lasing from single crystals of BP1T-CN. High group refractive index n_g (4.18–4.98) and high *Q* factor (910–1860) resulted in an efficient stimulated emission in the crystal cavity. Moreover, it was concluded that the extraordinary high material gain and high stimulated emission rate contributed to the lasing by means of pump-probe measurements. These results suggest that the BP1T-CN crystal has a promising potential as functional organic laser media.

Experimental Section

Sample Preparation: The synthesis and purification methods of BP1T-CN were carried out according to the published literature [4]. Crystallization of BP1T-CN was carried out by the following procedure. 5mg of BP1T-CN powder was placed in a glass tube and purged with N_2 gas at pressure of 170 mmHg. By heating at 330 °C for 30 h in a tube oven (Shibata GTO-350), rod-like crystals were obtained. The convection by the temperature gradient that arose from bottom to top of the glass tube gave rise to crystal nucleation sticking on the upper part of the glass tube wall. We selected a single crystal using a tungsten needle and attached it to a glass substrate to carry out the optical measurements. Fluorescence image of single-crystal BP1T-CN was taken under ultraviolet excitation (λ_{ex} = 365 nm) by using a fluorescence microscope (Olympus BX-51) with a 40× objective lens and a CCD camera (OLYMPUS DP21).

X-ray Diffraction (XRD): XRD analysis of the single crystal was carried out in the range of 2θ up to 50.7° at –150 ± 1 °C by using a RINT-TTRIII/NM (Rigaku). The Mo-Kα radiation (λ = 0.71075 Å) was used as the x-ray source.

Optical Measurements: We used a fluorescence spectrophotometer (JASCO FP-750) and a UV-VIS spectrophotometer (JASCO V-530) for absorption and PL measurements, respectively. For ASE and lasing measurements, the excitation beam (30 μm × 40 μm) was incident with an angle of 20° against the crystal plane. The light emitted from the crystal edges was collected with a CCD spectrometer (Roper Scientific ST-133 series). In the optical gain measurements, the integrated intensity of the 0-1 band ASE was measured as a function of excitation stripe lengths (0–800 μm). In the pump-probe measurements, a Ti:S femtosecond pulsed laser (Quantronix Integra λ_{ex} = 784 nm, 1 kHz, ~100 fs duration, 1.5 mJ output energy) was used as an optical source. The second harmonic of the output generated by a BBO crystal was used as an excitation light. A white laser beam generated by focusing the output of the Ti:S laser onto a 4 mm thick sapphire plate was used as a probe light for transient transmission spectroscopy.

Supporting Information

Supporting Information is available from the Wiley Online Library or from the author. CCDC-897042 contains the supplementary crystallographic data for this paper. These data can be obtained free of charge from The Cambridge Crystallographic Data Centre via www.ccdc.cam.ac.uk/data_request/cif.

Acknowledgements

This work was supported by Grant-in-Aid for Scientific Research on Innovation Areas from the Ministry of Education, Culture, Sports, Science and Technology of Japan (25286042). This work was also partly supported by the Green Photonics project of Nara Institute of Science and Technology. The authors gratefully acknowledge Dr. A. Ishizumi and Mr. S. Katao, Nara Institute of Science and Technology, Mr. M. Cadelano and Mr. V. Sarritzu, Dipartimento di Fisica, Università di Cagliari, for valuable discussions and experimental supports. The authors also acknowledge Prof. K. Ohmori, Institute for Molecular Science (IMS), National Institutes of Natural Sciences, for useful discussions.

Received: February 18, 2014
Revised: March 6, 2014
Published online: March 24, 2014

[1] M. Pope, H. P. Kallmann, P. Magnante, *J. Chem. Phys.* **1963**, *38*, 2042.
[2] S. Hotta, H. Kimura, S. A. Lee, T. Tamaki, *J. Heterocycl. Chem.* **2000**, *37*, 281.
[3] S. Hotta, T. Katagiri, *J. Heterocycl. Chem.* **2003**, *40*, 845.
[4] T. Katagiri, S. Ota, T. Ohira, T. Yamao, S. Hotta, *J. Heterocycl. Chem.* **2007**, *44*, 853.
[5] S. Kanazawa, M. Ichikawa, T. Koyama, Y. Taniguchi, *Chem. Phys. Chem.* **2006**, *7*, 1881.
[6] Y. Yomogida, T. Takenobu, H. Shimotani, K. Sawabe, S. Z. Bisri, T. Yamao, S. Hotta, Y. Iwasa, *Appl. Phys. Lett.* **2010**, *97*, 173301.
[7] T. Yamao, K. Juri, A. Kamoi, S. Hotta, *Organic Electronics* **2009**, *10*, 1241.
[8] H. Mizuno, U. Haku, Y. Marutani, A. Ishizumi, H. Yanagi, F. Sasaki, S. Hotta, *Adv. Mater.* **2012**, *24*, 5744.
[9] T. Yamao, K. Terasaki, Y. Shimizu, S. Hotta, *J. Nanosci. Nanotechnol.* **2010**, *10*, 1017.
[10] S. Hotta, M. Goto, R. Azumi, M. Inoue, M. Ichikawa, Y. Taniguchi, *Chem. Mater.* **2004**, *16*, 237.
[11] K. Bando, T. Nakamura, S. Fujiwara, Y. Masumoto, F. Sasaki, S. Shimoi, S. Hotta, *Phys. Rev. B* **2008**, *77*, 045205.
[12] K. Shimizu, Y. Mori, S. Hotta, *J. Appl. Phys.* **2008**, *99*, 063505.
[13] S. Hotta, M. Goto, R. Azumi, *Chem. Lett.* **2007**, *36*, 270.
[14] S. Hotta, Y. Shimizu, T. Yamao, M. Goto, R. Azumi, *Chem. Lett.* **2009**, *38*, 294.
[15] Y. Kawaguchi, F. Sasaki, H. Mochizuki, T. Ishitsuka, T. Tomie, T. Ootsuka, S. Watanabe, Y. Shimoi, T. Yamao, S. Hotta, *J. Appl. Phys.* **2013**, *113*, 083710.
[16] S. Nagamatsu, T. Moriguchi, T. Nagase, S. Oku, K. Kuramoto, W. Takashima, T. Okauchi, K. Mizoguchi, S. Hayase, K. Kaneto, *Appl. Phys. Express* **2009**, *2*, 101502.

[17] A. Yassar, F. Demanze, A. Jaafari, M. E. Idrissi, C. Coupry, *Adv. Funct. Mater.* **2002**, *12*, 699.
[18] T. Yamao, T. Miki, H. Akagami, Y. Nishimoto, S. Ota, S. Hotta, *Chem. Mater.* **2007**, *19*, 3748.
[19] T. Yamao, S. Ota, T. Miki, S. Hotta, R. Azumi, *Thin Solid Films* **2008**, *516*, 2527.
[20] S. Hotta, M. Goto, *Adv. Mater.* **2002**, *14*, 498.
[21] J. C. Ribierre, G. Tsiminis, S. Richardson, G. A. Turnbull, I. D. W. Samuel, H. S. Barcena, P. L. Burn, *Appl. Phys. Lett.* **2007**, *91*, 081108.
[22] H. Nakanotani, S. Akiyama, D. Ohnishi, M. Moriwake, M. Yahiro, T. Yoshihara, C. Adachi, *Adv. Funct. Mater.* **2007**, *17*, 2328.
[23] X. Liu, C. Py, Y. Tao, Y. Li, J. Ding, M. Day, *Appl. Phys. Lett.* **2004**, *84*, 2727.
[24] W. Holzer, A. Penzkofer, T. Schmitt, A. Hartmann, C. Bader, H. Tillmann, D. Raabe, R. Stockmann, H.-H. Hörhold, *Opt. Quantum Electron.* **2001**, *33*, 121.
[25] M. Anni, G. Gigli, R. Cingolani, M. Z. Rossi, C. Gadermaier, G. Lanzani, G. Barbarella, L. Favaretto, *Appl. Phys. Lett.* **2001**, *78*, 2679.
[26] T. Schwartz, J. A. Hutchison, J. Léonard, C. Genet, S. Haacke, T. W. Ebbesen, *Chem. Phys. Chem.* **2013**, *14*, 125.
[27] F. Cordella, F. Quochi, M. Saba, A. Andreev, H. Sitter, N. S. Sariciftci, A. Mura, G. Bongiovanni, *Adv. Mater.* **2007**, *19*, 2252.